

Generating function for projected entangled-pair states

Wei-Lin Tu,^{1,*} Laurens Vanderstraeten,^{2,3,†} Norbert Schuch,^{4,5,‡}
Hyun-Yong Lee,^{6,7,8,§} Naoki Kawashima,^{9,10,¶} and Ji-Yao Chen^{11,**}

¹*Faculty of Science and Technology, Keio University, 3-14-1 Hiyoshi, Kohoku-ku, Yokohama 223-8522, Japan*

²*Department of Physics and Astronomy, University of Ghent, Belgium*

³*Center for Nonlinear Phenomena and Complex Systems, Université Libre de Bruxelles, Belgium*

⁴*University of Vienna, Faculty of Physics, Boltzmannngasse 5, 1090 Wien, Austria*

⁵*University of Vienna, Faculty of Mathematics, Oskar-Morgenstern-Platz 1, 1090 Wien, Austria*

⁶*Division of Display and Semiconductor Physics, Korea University, Sejong 30019, Korea*

⁷*Department of Applied Physics, Graduate School, Korea University, Sejong 30019, Korea*

⁸*Interdisciplinary Program in E-ICT-Culture-Sports Convergence, Korea University, Sejong 30019, Korea*

⁹*Institute for Solid State Physics, University of Tokyo, Kashiwa, Chiba 277-8581, Japan*

¹⁰*Trans-scale Quantum Science Institute, The University of Tokyo, Bunkyo, Tokyo 113-0033, Japan*

¹¹*Center for Neutron Science and Technology, Guangdong Provincial Key Laboratory of Magnetoelectric Physics and Devices, School of Physics, Sun Yat-sen University, Guangzhou, 510275, China*

(Dated: July 18, 2023)

Diagrammatic summation is a common bottleneck in modern applications of projected entangled-pair states (PEPS), especially in computing low-energy excitations of a two dimensional quantum many-body system. To solve this problem, here we extend the generating function approach for tensor network diagrammatic summation, previously proposed in the context of matrix product states. With the excited state expressed as a one-particle excitation, we show that relevant objects in determining the variational parameters, i.e. effective hamiltonian and norm matrices in the variational parameter space can be easily computed in the generating function formalism, which can further be used in evaluating the dynamical structure factor. Our benchmark results for the spin-1/2 transverse field Ising model and Heisenberg model on the square lattice provide a desirable accuracy, showing good agreement with known results. Then we study the spin-1/2 $J_1 - J_2$ model on the same lattice and investigate the dynamical properties of the putative gapless spin liquid phase. We conclude with a discussion on generalizations to multi-particle excitations.

I. INTRODUCTION

Strongly correlated quantum systems play a central role in condensed matter physics, often triggering exotic behavior at low temperature. For systems in low dimensions where quantum effects are manifest, it is nowadays widely acknowledged that the entanglement based tensor network method serves as an ideal tool for both analytical and numerical studies of these systems [1, 2]. Apart from its huge success in investigating the properties of ground states due to its area-law-fulfilling structure, the low-energy properties above the ground state such as dynamical correlations and entanglement dynamics can also be studied. The former are often directly measurable in spectroscopic experiments of condensed matter physics, e.g., inelastic neutron scattering experiments in quantum magnets [3], whereas out-of-equilibrium properties can be accessed in quantum simulators [4]. However, in more than one spatial dimension, progress towards a complete understanding of the low-energy excitations in a quantum many-body system in terms of tensor networks is still at its infancy. Thus, an efficient and accurate way of computing low-lying

excitations and associated dynamical correlation functions for two dimensional (2D) systems is highly desired.

With numerous efforts in the last twenty years, projected entangled-pair states (PEPS) have now become one of the cornerstones for studying 2D quantum many-body systems [5]. Along with the better understanding of its mathematical structure and improved numerical recipes, PEPS has been shown to capture ground states of many important classes of two-dimensional phases of matter, including non-chiral topological states [6–9], ordered quantum magnets [10–16], (chiral) quantum spin liquids [17–22], and various phases in fermionic systems [23–27]. Beyond ground state properties, the PEPS toolbox has been extended to capture excited states [28–32], time evolution [33–38] and finite temperature properties [39–45]. Compared to ground state search with PEPS, which has become almost mature, the latter developments are still quickly evolving. It is therefore natural and promising to further develop theoretical tools to extend the success for ground states to excitations of 2D systems with PEPS.

One physically motivated way of studying excitations is to use the tensor network generalization [46, 47] of the Feynman-Bijl ansatz [48–51] or single mode approximation [52, 53], which is a variational ansatz for an excited state in the tangent space of the ground state tensor manifold [54, 55]. In this construction, the ground state is perturbed locally by introducing an “impurity” tensor (orthogonal to the ground state) to represent a local quasiparticle. By making a momentum superposition of such a local perturbation, one obtains a natural representation for a low-energy excited state. This approach has been successfully applied to build excita-

* weilintu@keio.jp

† laurens.vanderstraeten@ugent.be

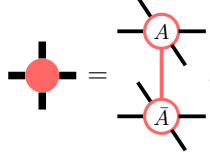
‡ norbert.schuch@univie.ac.at

§ hyunyong@korea.ac.kr

¶ kawashima@issp.u-tokyo.ac.jp

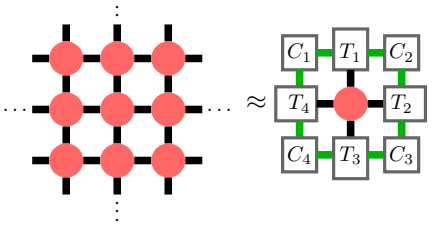
** chenjiy3@mail.sysu.edu.cn

where



$$(3)$$

The thick black bonds in Eq. (3) thus have dimension D^2 . Through the CTMRG procedure, one can obtain a series of environment tensors which serve as the approximation of all surrounding tensors:



$$(4)$$

Here, the C_i tensors are the corner tensors and the T_i 's stand for the edge tensors ($i = 1, 2, 3, 4$). The green bonds (bonds that connect C and T tensors) possess dimension equal to χ and typically one would choose $\chi \geq D^2$ to ensure the results are not affected by finite environment bond dimension. Note that, to obtain the environment tensors, one would need to introduce projectors to truncate the growing environment bond dimension. Apart from the ground state calculation, we will show that the environment tensors and the projectors will play an important role also in the calculations of generating functions.

With these environment tensors, the reduced density matrix of a certain number of local sites can be constructed and the energy can be evaluated. Given a local Hamiltonian of the form $H = \sum_i h_i$, the energy density can be calculated as

$$e = \frac{\langle \Psi(A) | h_i | \Psi(A) \rangle}{\langle \Psi(A) | \Psi(A) \rangle}. \quad (5)$$

Note that, when computing Eq. (5), the approximations due to projectors in CTMRG are the same for the numerator and denominator. This point will be illuminating when considering contraction scheme for generating functions of PEPS.

The remaining task lies in the optimization of the ground state tensor A to minimize the variational energy, which conventionally can be done through imaginary time evolution where the local Hamiltonian is used to construct Suzuki-Trotter gates, and after a long enough evolution a well approximated ground state ansatz can be obtained [70, 79, 80]. However, the initial ansatz for imaginary time evolution tends to significantly affect the final outcome, hindering the simulation without any tentative knowledge of the target model and sometimes causing a serious issue of getting trapped in the local minima of Hilbert space. Additionally, due to the approximations involved in truncating the PEPS after applying Suzuki-Trotter gates, the imaginary time evolution does not always converge to the variationally optimal PEPS tensor.

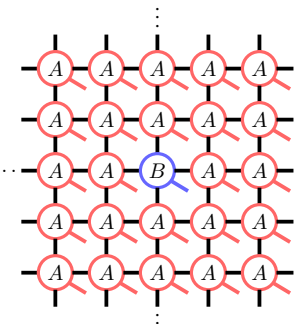
Instead of doing imaginary time evolution, directly minimizing the energy through energy gradient, i.e. variational optimization, has proven to be a more accurate optimization scheme [81, 82]. When the number of variational parameters is small (for example, when the PEPS tensors are strongly constrained by symmetries), variational optimization can be done using a simple finite difference approach to compute the energy gradient [19, 20, 83, 84]. For generic tensors, a direct evaluation of the gradient requires a summation of large number of tensor diagrams to evaluate the final gradients [72, 81, 82], but the numerical derivatives can be evaluated through automatic differentiation (AD) [85]. By storing the computational graph of PEPS [14, 15] in the memory during the forward-mode calculation, the numerically exact gradients can be evaluated through the back propagation [86]. We then make use of those gradients to further optimize our tensors in order to lower the ground state energy.

In the following simulations, we have checked that for each bond dimension D the chosen value of χ is either large enough and the results barely change with even larger χ , or the largest within the computational capacity. In searching of the ground state, we also adopt the tensor with C_{4v} symmetry on the square lattice due to the existence of the rotational symmetry in our target states.

B. Quasiparticle excitation with PEPS

The excited state for a given many-body Hamiltonian can be thought of as a quasiparticle excitation on top of the ground state [87]. As mentioned in the introduction, in real space such an excitation can be approximated through the tensor network version of the single mode approximation, where we replace one ground state tensor with some ‘‘impurity’’ tensor at a certain location [88]. We then sum up all different tensor network configurations generated by the translation operator, multiplied by the corresponding phase factors in the front to build an eigenstate of translation operator with a given momentum.

With the ground state expressed as a one-site translation invariant iPEPS, the one-particle excitation with PEPS can be written as:



$$|\Phi_{\mathbf{k}}(B)\rangle = \sum_{\mathbf{r}} e^{-i\mathbf{k} \cdot \mathbf{r}} \hat{T}^{\mathbf{r}} \dots, \quad (6)$$

where \hat{T} stands for the translation operator with its eigenvalue being $e^{i\mathbf{k}}$, and B is the impurity tensor to be determined.

Due to linear dependence of excited states on the impurity

tensor, the variational optimization boils down to a generalized eigenvalue problem

$$\mathbf{H}_{\mu\nu} B_\nu = \mathbf{E} \mathbf{N}_{\mu\nu} B_\nu, \quad (7)$$

where \mathbf{H} and \mathbf{N} are the effective Hamiltonian and norm matrices in the variational space. With the translation invariance, \mathbf{N} can be obtained by hollowing out the \bar{A} tensor in the center of the bra layer, and the summation goes through every tensor graphs with an empty site in the ket layer. Using channel operators with boundary MPS [28], this sum can be carried out at the same computational cost of ground state computation. A slightly different summation scheme using CTMRG has also been proposed in Ref. [30]. Similarly, the effective Hamiltonian \mathbf{H} can also be computed, where an additional summation for the Hamiltonian operator appears. These summations are the main bottleneck of studying excitations using the quasi-particle ansatz.

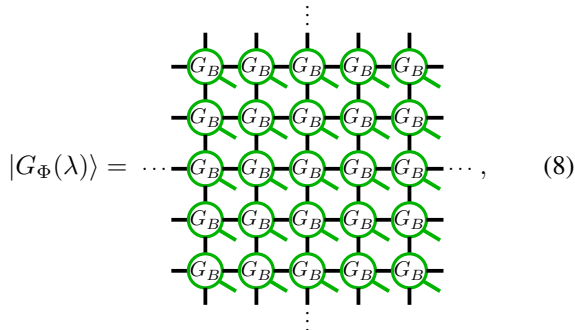
Because of the gauge freedom in the PEPS representation [Eq. (1)] in terms of the local tensor A , the linear subspace of excitations contains a few zero modes [28]. These are reflected as zero eigenvalues in the effective norm matrix, and should be projected out to make the above eigenvalue equation well-conditioned. We will come back to the conditioning of \mathbf{N} below.

III. THE GENERATING FUNCTION

A. Algorithm

The issue of summing up many diagrams also appear in the MPS study of 1D quantum system, where some of the authors and collaborators have proposed generating functions to tackle this [64]. Now we adopt this method in the current setting of PEPS in the thermodynamic limit. The basic idea of generating function is that the sum of extensive tensor diagrams can be expressed as a low-order derivative of a new tensor diagram. This was possible for excited states due to the fact that tensor diagrams only differ by the location of the impurity tensor.

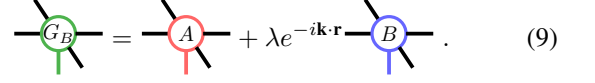
For infinite PEPS, following Ref. [64], we define the generating function for the one-particle excited state as



$$|G_\Phi(\lambda)\rangle = \dots \quad (8)$$

where G_B stands for the generating function of the impurity

tensor and takes the following position-dependent form:



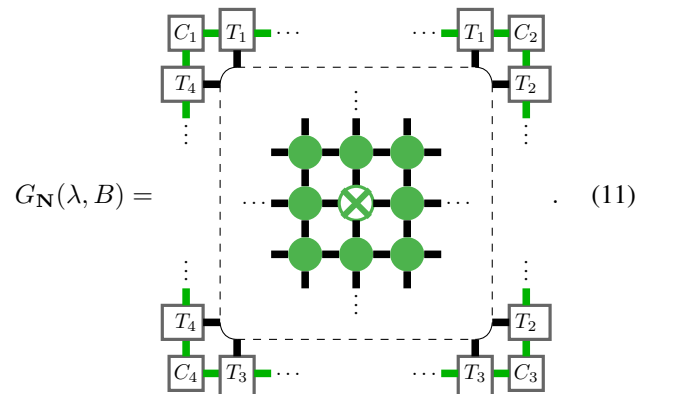
$$G_B = A + \lambda e^{-i\mathbf{k} \cdot \mathbf{r}} B. \quad (9)$$

The one-particle excited state in Eq. (6) can now be evaluated by taking the derivative

$$|\Phi_{\mathbf{k}}(B)\rangle = \frac{\partial}{\partial \lambda} |G_\Phi(\lambda)\rangle \Big|_{\lambda=0}. \quad (10)$$

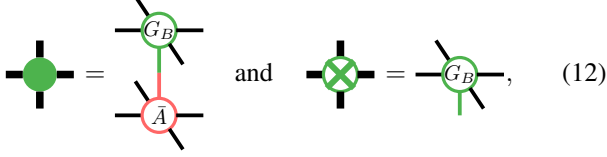
One question immediately follows. Namely, what would be the right environment tensors for $\langle G_\Phi(\lambda) | G_\Phi(\lambda) \rangle$ when computing physical observables. Note that, for PEPS in the thermodynamic limit, the contraction scheme relies on the translation invariance to interpret the environment tensors as fixed points of the one dimensional transfer operator. For the generating function Eq. (8), this translation invariance is lost for any nonzero λ . The solution of this issue comes from the following fact: after taking derivatives at $\lambda = 0$, all contributions of the sum can be viewed as correlation functions of local operators. Recalling that when computing observables or correlation functions in the infinite MPS, one use the fixed point of the transfer matrix as the boundary, suggesting that fixed point tensors of transfer matrix of the ground state infinite MPS are the right environment tensors for generating function of infinite MPS. The same is true for ground state PEPS in the thermodynamic limit. Indeed, we have tested that using fixed point of MPS transfer matrix in the generating functions gives the same result as directly summing all tensor diagrams. Thus, similarly for PEPS, we can use the environment tensors from CTMRG of ground state PEPS (i.e., the state $|G_\Phi(\lambda)\rangle$ at $\lambda = 0$) as the environment tensors for the generating function Eq. (8).

With the generating function for the excited state, the norm matrix and effective Hamiltonian can be similarly expressed as derivatives of a single network. Using translation symmetry, we can lower the order of derivatives by introducing two slightly new networks [64]. For that, we first construct two (idealized) generating functions, $G_{\mathbf{N}}(\lambda, B)$ and $G_{\mathbf{H}}(\lambda, B)$ for norm matrix and effective Hamiltonian, respectively. $G_{\mathbf{N}}$ takes the following form:



$$G_{\mathbf{N}}(\lambda, B) = \dots \quad (11)$$

The green tensors in Eq. (11) are given by

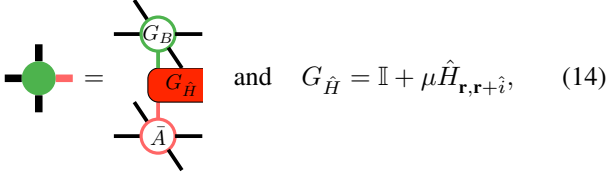


$$\text{Green tensor with cross} = \text{Green tensor with cross and red circle} \quad \text{and} \quad \text{Green tensor with cross} = \text{Green tensor with cross and green circle}, \quad (12)$$

where the tensor with cross mark lies in the center of the lattice. The norm matrix can then be evaluated by taking the derivative,

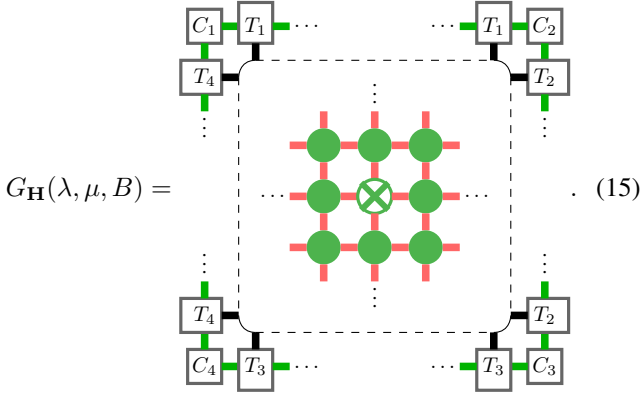
$$\mathbf{N} = \frac{\partial}{\partial B} G_{\mathbf{N}}(\lambda, B) \Big|_{\lambda=1, B=0}. \quad (13)$$

For the generating function of the effective Hamiltonian, we need to insert the Hamiltonian in between the bra layer and the ket layer. Note that, although the local Hamiltonian can be represented as a projected entangled-pair operator, it is rarely used in practice, due to the increased computational cost. Here we use the generating function for a local Hamiltonian, as introduced in Ref. [64], to represent the full Hamiltonian as a derivative of a new network. Then we sandwich the generating function of the local Hamiltonian term between the bra and ket layers. To illustrate, assuming that we only have the nearest neighbor terms, a new tensor can be defined as:



$$\text{Green tensor with cross} = \text{Green tensor with cross and red circle} \quad \text{and} \quad G_{\hat{H}} = \mathbb{I} + \mu \hat{H}_{\mathbf{r}, \mathbf{r}+\hat{i}}, \quad (14)$$

where \mathbb{I} is the identity matrix and $\hat{i} = \hat{x}, \hat{y}$. Then the (idealized) generating function for the effective Hamiltonian is given by the following:



$$G_{\mathbf{H}}(\lambda, \mu, B) = \text{Diagram of the generating function} \quad (15)$$

From Eq. (15), the effective Hamiltonian \mathbf{H} can be obtained by taking a second order derivative

$$\mathbf{H} = \frac{\partial^2}{\partial B \partial \mu} G_{\mathbf{H}}(\lambda, \mu, B) \Big|_{\lambda=1, \mu=0, B=0}. \quad (16)$$

Denoting the linear size of the bulk, i.e., the region encircled by dashed box in Eqs. (11) and (15), as L_x and L_y , it appears that L_x and L_y have to be chosen carefully. In

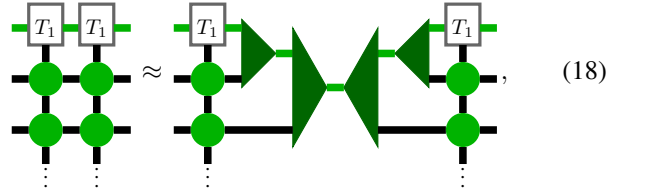
the case of infinite MPS, we have checked that the linear size in the bulk has to be compatible with the momenta, i.e., $k = 2\pi m/L_x$ ($m = 0, 1, 2, \dots, L_x - 1$), to ensure exact zero modes in the norm matrix. We expect the same is also true in the two dimensional case. Moreover, L_x and L_y should be large enough (compared to the correlation length of the ground state) to mimic an infinite system, so that the error due to finite linear size becomes negligible. At the same time, with larger linear size more \mathbf{k} points can be considered.

With the effective norm and Hamiltonian matrix obtained from derivatives of generating functions, we can now solve the generalized eigenvalue equation in Eq. (7), and obtain the impurity tensor \mathbf{B} for excited states. As mentioned before, due to gauge degree of freedom, exact zero modes appears in the norm matrix and one needs to project out the corresponding subspace, leading to the following generalized eigenvalue equation:

$$(P^\dagger \mathbf{H} P)_{\mu\nu} \mathbf{B}_\nu = E (P^\dagger \mathbf{N} P)_{\mu\nu} \mathbf{B}_\nu, \quad (17)$$

where the projector P projects out the exact zero modes of norm matrix. Note that, up to this point, there is no approximation involved and the scheme can be directly applied to the infinite MPS context where computation can be made essentially exact.

However, there is one more issue for PEPS to address: for large tensor network graphs in 2D (Eqs. (11), (15)), its computational complexity grows exponentially with system size. Therefore, the exact contraction is not feasible. By utilizing the projectors during the CTMRG process, on the other hand, we can approximate tensors on each column (row) as the following:



$$\text{3x3 grid of green tensors} \approx \text{Single green tensor with projectors} \quad (18)$$

where the projectors can be evaluated through the singular value decomposition [23] and a similar process can be conducted for the row and corner tensors. With the projectors inserted, now we show the complete tensor network for the norm matrix in Fig. 1. Note that here we demonstrate how to compress our tensor graphs vertically but in fact the similar action is taken along the horizontal direction. We can then take the average of these two compressed tensor graphs as $G_{\mathbf{N}}(\lambda, B)$.

For $G_{\mathbf{H}}(\lambda, \mu, B)$, we need to insert the generating function of $\hat{H}_{\mathbf{r}, \mathbf{r}+1}$ in between the bra and ket layers. In practice, since we make use of the projectors to compress the tensor graphs, the calculation is conducted twice; that is to say, we include $G_{\hat{H}}$ in all the vertical (horizontal) bonds and compress the tensor graph for each column (row).

The scheme is now clear and all we need to do is to first contract the *finite* tensor network in Eqs. (11) and (15) (with projectors inserted), and then compute the derivatives using either AD or any other way of numerical finite difference approach. Then, by solving the eigenvalue equation Eq. (17) af-

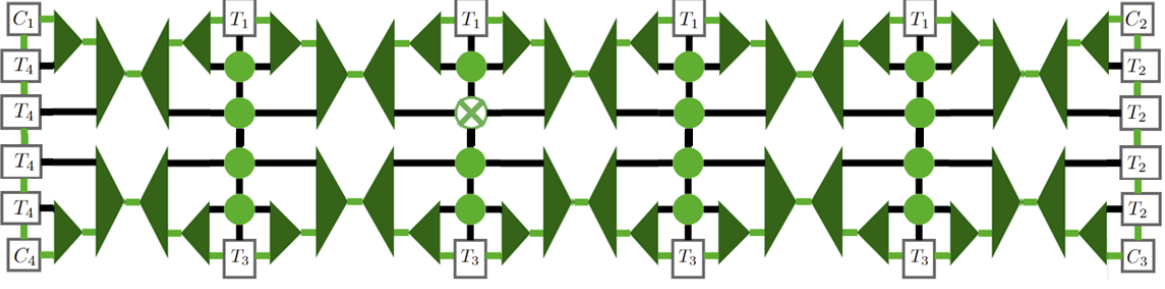


FIG. 1. Complete tensor network for generating function of norm matrix with $N_s = 4 \times 4$. The projectors inserted are taken from the CTMRG of the ground state. Similarly for the generating function of the effective Hamiltonian.

ter getting \mathbf{N} and \mathbf{H} , we then obtain the impurity tensors with corresponding energies.

Note that, due to the projectors inserted in Fig. 1, the zero modes in the norm matrix are no longer exact, and instead become fuzzy. Therefore, we adopt the projector P to reduce the basis and discard the subspace vectors whose norm matrix eigenvalues are too close to zero [30]. Denoting the eigenvalue decomposition of \mathbf{N} as $\mathbf{N} = v\Lambda v^\dagger$, we keep the desired subspace of v and construct \tilde{v} , which serves as P in Eq. (17). One thing to be mentioned here is that the selection of subspace cannot be simply defined. We start from the largest eigenvalue and gradually enlarge the size of subspace. If the inclusion of one vector makes the energy values change drastically, we then neglect this vector when constructing the subspace. After the above measures, we solve Eq. (17) and the excited state can then be constructed with \mathbf{B}_ν for further investigation of its properties.

B. Discussion of the algorithm

Comparing to the previous generating functions for finite sized MPS [64], two new ingredients are included in the infinite PEPS case. The first one is the concerning the infinite size in typical PEPS calculations. Although our scheme can be easily generalized to the finite PEPS, due to large computational cost, iPEPS is typically used in the literature. For that purpose, we have introduced ground state environment tensors in the effective norm and Hamiltonian matrices.

The second ingredient is about the contraction of the generating functions, where we have used ground state projectors to achieve an efficient contraction. The idea of using projectors from the ground state CTMRG procedure can further be put on firm grounds as follows. Notice that all the correlations are essentially mediated by the ground state tensors and all contributions to the effective Hamiltonian and norm matrix can be viewed as correlation functions of local operators in the ground state. Unravelling the CTMRG procedure, one would find that the CTMRG procedure is essentially inserting projectors (which was computed self-consistently) into the original network. Therefore, it is natural to use the same projectors when computing the generating function for excitations. We also note that, this scheme is not restricted to CTMRG

and in fact can be generalized to any other PEPS contraction methods, e.g., tensor renormalization group [75] and boundary MPS approach [70].

In comparison with previous approaches using PEPS for the construction of one-particle excited state, our approach largely reduces the number of tensor diagrams to be considered. In Ref. 28 the tensor contraction is done by evaluating the corner-shaped transfer matrix, with norm matrix and effective Hamiltonian obtained by summing up the tensor diagrams whose impurity tensors in the bra and ket layer are located in different relative positions. While the corner transfer matrices are also adopted in Ref. [30] for the environment tensors but again due to the position change many tensor graphs need to be taken into account.

The approach proposed in Ref. 31 comes closer to the approach presented here, which relies on AD to do the tensor diagram summations. Let us now compare with that one here. The most prominent feature of our approach is that we only need to deal with one tensor diagram for $N_{\mu\nu}$ or $H_{\mu\nu}$, where all the tensors are fixed before contraction. In Ref. 31, one needs to take care of the additional environment tensors (coming from impurity tensors), which were computed iteratively. In this sense, the approach presented here gets rid of all the intricate summations and updating steps in PEPS excitations. This simplification will play an essential role when considering multi-particle excitations with PEPS.

Before showing the applications, let us also mention that the usage of generating functions are in fact independent of AD. In some cases, the derivative is taken only with respect to one parameter λ and therefore can be easily done using finite difference method. In fact, using finite difference may become crucial when the bond dimension is large, since in that case the AD might be limited to memory issues. Nevertheless, in this work we use AD to reduce error and leave other possibilities for future works.

IV. APPLICATIONS

Now we benchmark our algorithm with two well-studied models, namely the transverse-field Ising model and spin-1/2 Heisenberg model on the square lattice, and then move to the more challenging $J_1 - J_2$ model.

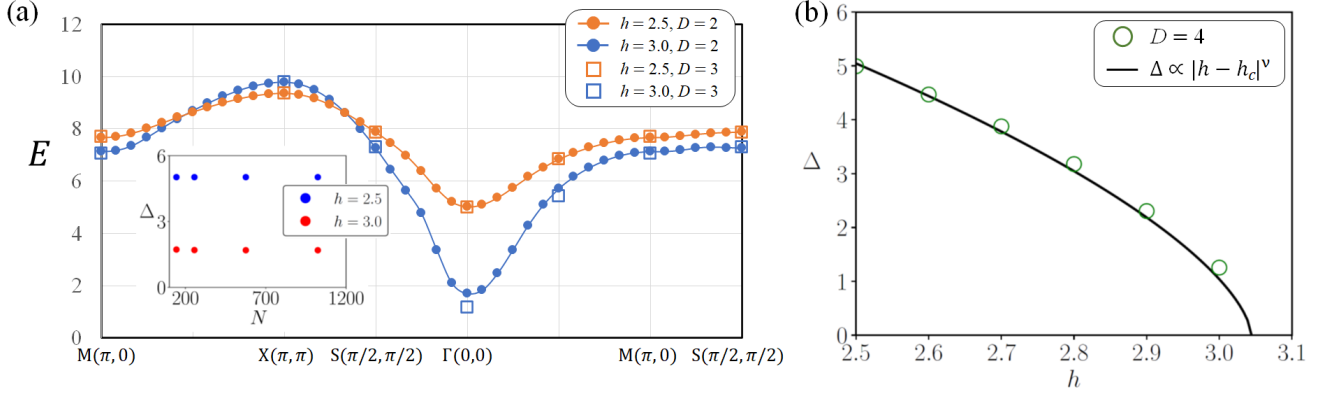


FIG. 2. (a) The energy dispersion for the lowest-lying excitation of transverse field Ising model at distinct k points for $h = 2.5$ and $h = 3.0$. We adopt $N_s = 24 \times 24$ for $D = 2$ and $N_s = 16 \times 16$ for $D = 3$ and confirm that further enlarging N_s does not change the results. The inset shows the energy gap with different N_s . (b) The gap function along with magnetic field h . We adopt $D = 4$ and $N_s = 12 \times 12$, while the solid curve fulfills the scaling relation for 3D Ising universality class with the critical exponent $\nu = 0.629971$.

A. Transverse field Ising model

The spin-1/2 quantum Ising model with a transverse field in 2D is described by

$$H_{\text{TFI}} = - \sum_{\langle i, j \rangle} \sigma_i^z \sigma_j^z - h \sum_i \sigma_i^x, \quad (19)$$

where $\sigma^{x,z}$ are the Pauli matrices and the summation of $\langle i, j \rangle$ concerns all nearest neighbor sites. As the most widely known model for benchmark, its phase transition can be accurately captured by PEPS [70, 89], and the most reliable approximation of its transition point was made by the cluster Monte Carlo method with the value being $h_c = 3.04438$ [90]. When $h \rightarrow \infty$, the ground state enjoys the global \mathbb{Z}_2 symmetry $\hat{U} = \prod_i \sigma_i^x$ with a non-zero energy gap. On the other hand, as $h = 0$ the ground state possesses a two-fold degeneracy with spins aligning all up or all down, which breaks the \mathbb{Z}_2 symmetry. Close to the transition point, the energy gap diminishes and becomes zero at h_c , which is a Lorentz-invariant criticality.

In order to compare with the results in Refs. [29] and [30], we first solve for the lowest-energy excited state and plot its dispersion in Fig. 2(a). From the results, one can find that away from the critical point ($h = 2.5$), the finite D effect is rather small, as the excitation energy does not show significant changes from $D = 2$ to $D = 3$. For magnetic field h close to the critical point ($h = 3.0$), the finite D effect only shows up in the smallest excitation energy point. While our results show qualitative and quantitative agreement, we can also see that the energy gap, Δ , decreases with larger bond dimension at the $\Gamma(0, 0)$ point. To make sure that the results are not sensitive to the choice of different bulk system size, we show the energy gap with various $N = L_x \times L_y$ for $D = 2$ as an inset of Fig. 2(a). It can be clearly seen that Δ barely changes as long as the size is large enough.

Since the continuous phase transition of the transverse-field Ising model concerns the breaking of \mathbb{Z}_2 symmetry, its universality class belongs to the 3D Ising as we are consider-

ing the zero-temperature quantum limit here. As a result, one further check that we can do is to generate the Δ - h dependence, which is ought to scale under the critical exponent ν . In Fig. 2(b) we provide the gap function with $D = 4$, and plot the analytical scaling of $\Delta \propto |h - h_c|^\nu$. One can see that indeed the gap function obtained by PEPS produces a desirable accuracy.

B. Heisenberg model

Next, we examine another model widely used for the purpose of benchmarking, the antiferromagnetic (AFM) Heisenberg model:

$$H_{\text{Heisenberg}} = J \sum_{\langle i, j \rangle} \mathbf{S}_i \cdot \mathbf{S}_j, \quad (20)$$

where we take $J = 1$ as the energy unit, and the sum runs over all nearest-neighbor pairs. While the AFM nature demands at least a 2×2 unit cell for the ground state ansatz, by rotating the local spin on one sublattice we can still preserve the one-site translation symmetry for PEPS.

Before showing the excited states, as a good benchmark we first compute the static structure factor, which can be measured by elastic neutron scattering experiments. The static structure factor is defined by the following equation [91]:

$$S(\mathbf{k}) = \sum_{\mathbf{r}, \alpha} e^{i\mathbf{k} \cdot \mathbf{r}} \langle S_0^\alpha S_{\mathbf{r}}^\alpha \rangle_c = \sum_{\alpha} S^\alpha(\mathbf{k}), \quad (21)$$

where $\langle \cdot \rangle_c$ denotes the connected part of the correlator and $\alpha = x, y, z$. Because of the antiferromagnetic nature the static structure factor possesses a peak at $\mathbf{k} = (\pi, \pi)$, while it becomes zero at $\mathbf{k} = (0, 0)$. Given a variational PEPS ground state, using generating functions such a two-point correlation function can easily be evaluated. We calculate $S(\mathbf{k})$ with $D = 4$ in Fig. 3. Our result is in good agreement with the previous one using iPEPS [81], as well as those by other

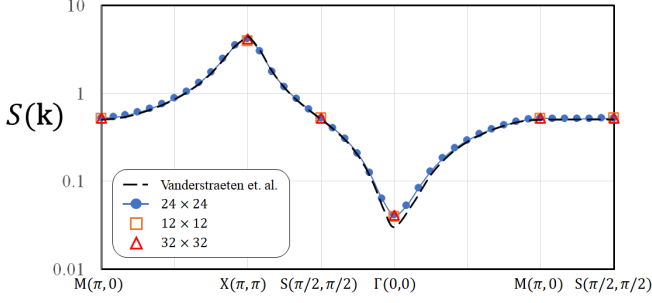


FIG. 3. Static structure factor $S(\mathbf{k})$ for the Heisenberg model ($D = 4$), with three different N_s . For comparison, the black dashed line shows the results of Ref. [81] with $D = 4$.

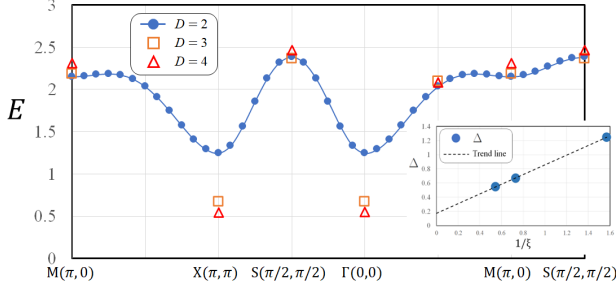


FIG. 4. The lowest energy excited state dispersion for Heisenberg model with $D = 2$ ($N_s = 24 \times 24$), 3 ($N_s = 16 \times 16$), and 4 ($N_s = 12 \times 12$). The inset shows the scaling of Δ with inverse of correlation length, $1/\xi$. As $\xi \rightarrow \infty$, Δ extrapolates to a value close to zero.

methods [91, 92]. More importantly, results of different N_s all look similar, fortifying the fact that for our method the choice of bulk size casts little effect in the final outcomes.

In Fig. 4 we show our results for the lowest-energy dispersion of the Heisenberg model. One clear feature we can see lies in the vanishing of Δ along with D , which is desirable because the Heisenberg model is known to be gapless with a linear dispersion near the $\Gamma(0, 0)$ and $X(\pi, \pi)$ points. To further confirm the gapless nature, in the inset we provide the scaling of Δ with $1/D$. We can see that the energy gap indeed extrapolates to a small value when $D \rightarrow \infty$. Except for the gapped feature due to the finite bond dimension, our dispersion is very similar to the ones by earlier iPEPS results [29, 30] and Gutzwiller-projected trial wavefunctions [93]. Also, the well-known feature that the gap at $(\pi, 0)$ is smaller than the one at $(\pi/2, \pi/2)$ [93] is recovered in our simulation. In fact, the nature around $M(\pi, 0)$ point is of interest and has been under investigation [94–96]. In Ref. [30] it has been demonstrated using PEPS that the repulsion from the multi-magnon branches pushes the magnon at $M(\pi, 0)$ to a lower energy [95]. This feature has also been captured in our simulation by showing a dip in the single magnon energy branch near the M point. In the next section we will show that after introducing the next-nearest-neighbor (NNN) J_2 coupling the energy gap at $M(\pi, 0)$ is further reduced. Curiously, we find that the excitation energy at the M point goes up slightly as

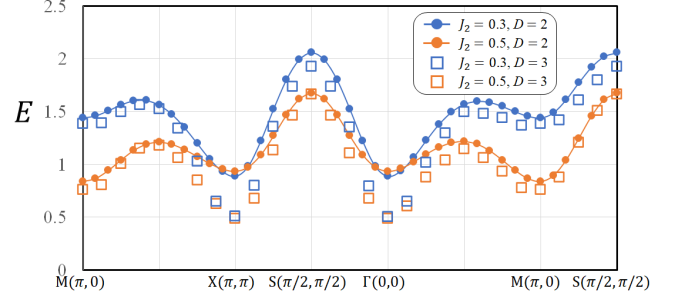


FIG. 5. The energy dispersion for the lowest excited state of the $J_1 - J_2$ model at distinct k points for $J_2 = 0.3$ and $J_2 = 0.5$. We adopt $N_s = 24 \times 24$ for $D = 2$ and $N_s = 16 \times 16$ for $D = 3$.

we increase the bond dimension D , which could be due to the various approximations in our approach; we leave a further investigation of this effect for future work.

C. Spin-1/2 J_1 - J_2 antiferromagnet

In the previous sections, we have studied models with only nearest neighbor couplings using our method. Both the transverse field Ising model and Heisenberg model have served as good benchmarks and have been studied earlier using conventional iPEPS construction for excited states [28–31]. Here, we aim to push further and study the $J_1 - J_2$ model where the next-nearest-neighbor coupling introduces frustration and thus exotic underlying states [97, 98]. The Hamiltonian is given by:

$$H_{J_1 - J_2} = J_1 \sum_{\langle i, j \rangle} \mathbf{S}_i \cdot \mathbf{S}_j + J_2 \sum_{\langle\langle k, l \rangle\rangle} \mathbf{S}_k \cdot \mathbf{S}_l, \quad (22)$$

where the J_1 (J_2) term runs over all (next-)nearest-neighbor pairs on the square lattice.

The $J_1 - J_2$ model has been under intense investigation: since the frustration induces a sign problem for quantum Monte Carlo methods, alternative numerical methods have been applied, suggesting that between $J_2 \approx 0.5$ and $J_2 \approx 0.6$ a ground state without magnetic order is realized (hereafter we fix $J_1 = 1$). Using PEPS methods, this vanishing of the staggered magnetization has been confirmed [14] using advanced scaling techniques – for any finite bond dimension, it appears that a variational PEPS ground state yields a non-zero magnetization. Here we will now investigate the excitation spectrum for this frustrated model.

In order to include the NNN coupling, \hat{i} in Eq. (14) now represents \hat{x} , \hat{y} , $\hat{x} + \hat{y}$, and $\hat{x} - \hat{y}$. As a result, the tensor contraction one needs to apply when preparing G_H becomes cumbersome. For example, the tensor graphs that we need to consider now

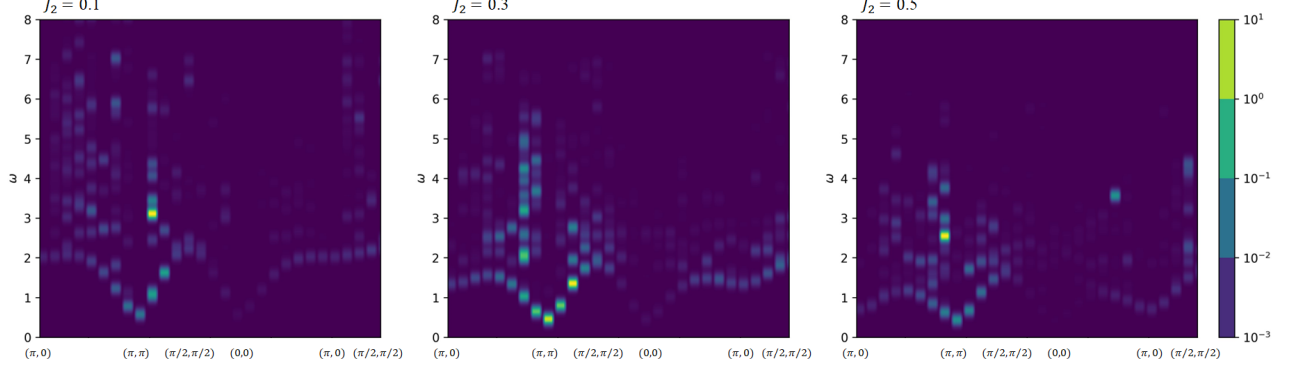


FIG. 6. The dynamical structure factor for J_1 - J_2 model with $D = 3$. Here we show results for $J_2 = 0.1$ (left panel), $J_2 = 0.3$ (middle panel), and $J_2 = 0.5$ (right panel), with $N_s = 16 \times 16$. We replace the delta function with normalized Gaussian broadening with width $\sigma = 0.1$.

involve two columns at the same time:

This consumes more memory when storing the computational graph for the back propagation. Therefore, our calculation in this work is restricted to $D = 3$ for the $J_1 - J_2$ model and we will leave the further consideration on enlarging the available bond dimension for future work.

In Fig. 5 we show the lowest-energy quasiparticle dispersion for the $J_1 - J_2$ model with $J_2 = 0.3$ and $J_2 = 0.5$ along a high symmetry path in the Brillouin zone. Similar to the case for the Heisenberg model, when the bond dimension increases the energy gap becomes smaller, in agreement with the phase being gapless [99]. Moreover, these dispersions also look similar to those by a variational Monte Carlo (VMC) method [100]. Besides the shape of the dispersion, we can clearly see that the energy gap becomes smaller at $M(\pi, 0)$ when J_2 increases. More importantly, at $J_2 = 0.5$ our results using $D = 2$ indicate that even the $M(\pi, 0)$ point becomes gapless. This softening of the dispersion at the M point is suggestive of the formation of a spin liquid phase at intermediate values, where the mode at the M point would correspond to a two-spinon state [100].

Based on the variational wavefunctions for the excited states, it is straightforward to compute their contributions to the dynamical structure factors. In Fig. 6, we show the dynamical spin structure factor for $J_2 = 0.1, 0.3, 0.5$, respectively, where all data are computed with PEPS bond dimension $D = 3$. Two clear features can be seen from our data: (1) the energy gap gets softened at the $M(\pi, 0)$ point, and (2) the spectral weights gets closer to the magnon branch (lowest excited energies) in the frustrated region. We have noted that in the previous results by VMC the authors also observed the similar trend in their dynamical structure factor, where a clear energy continuum is formed after $J_2/J_1 \approx 0.45$. Although

the resolution in our results is not clear enough, we expect to see a possible energy continuum after pushing to a larger D with a suitable method for scaling the results.

V. CONCLUSION

In this work, we have extended the generating functions introduced in Ref. 64 to PEPS. After obtaining the well approximated ground state through variational optimization, we solve the eigenvalue problem in Eq. (17) where effective Hamiltonian and norm matrices are evaluated by taking the derivatives of their corresponding generating functions. We then utilize the eigenstates as the impurity tensors to construct the one-particle excited state and employ the transverse field Ising model and Heisenberg model as benchmarks. Our results demonstrate good consistency with previous ones [29, 30] using PEPS where the serial summation on different parts of tensor graphs is needed. We extend our consideration to the model with NNN coupling and study the $J_1 - J_2$ model. Despite the increasing computational cost which hinders the computation with larger D , our results already show good agreement with previous ones by VMC.

Before closing, let us discuss how to generalize this idea to multi-particle excitations, especially those associated with spinons. It is known that spin liquids are characterized by fractionalized excitations, where the quasiparticles cannot appear alone, but come in pairs, which are intrinsically two-particle excitations. In the previous study, spinon excitation (among other fractional excitation) have been treated in MPS calculation using quantum numbers, which appears as a local excitation with a non-local string attached [101, 102]. In the case of PEPS, fractionalized excitations can also be defined and their static properties, e.g., correlation functions and correlation lengths have been studied in Ref. [20]. In that case, the local tensor of PEPS needs a certain gauge symmetry. Once constructed, the excited states containing spinon excitations can be obtained. To further study dispersion relation of spinon excitation, one may put one spinon at infinite far away, or, using a suitable boundary condition, to reduce

the problem into an effective one-particle problem. Generating functions can then be used for efficiently optimizing the one-particle problem as we have shown above.

In summary, our proposal of combining the generating function with tensor network ansatz helps reduce the complexity in obtaining the physical properties or observables concerning the summation of tensor networks. We are looking forward to seeing more applications, such as generalized multi-particle excitations.

Note added — When finalizing this work, we became aware of a related work using AD methods for diagram summations in PEPS [103].

Acknowledgments — We acknowledge discussions with Ying-Jer Kao, Tsuyoshi Okubo, and Jens Eisert. Authors also acknowledge the Advanced Study Group (ASG) *Tensor Network Approaches to Many-Body Systems* organized by the Center for Theoretical Physics of Complex Systems (PCS) of the Institute for Basic Science (IBS) in Daejeon, Korea. Part of the calculation in this work was conducted in the Su-

percomputer Center of ISSP, the University of Tokyo. W.-L.T. is supported by the Center of Innovations for Sustainable Quantum AI (JST Grant Number JPMJPF2221). H.-Y.L. is supported by National Research Foundation of Korea under the grant numbers NRF-2020R1I1A3074769 and Basic Science Research Program through the National Research Foundation of Korea (NRF) funded by the Ministry of Education (2014R1A6A1030732). N.K. is supported by JSPS KAKENHI Grants No. JP19H01809 and No. JP23H01092. J.-Y.C. was supported by Open Research Fund Program of the State Key Laboratory of Low-Dimensional Quantum Physics (project No. KF202207), Fundamental Research Funds for the Central Universities, Sun Yat-sen University (project No. 23qnp60), a startup fund from Sun Yat-sen University (No. 74130-12230034), and the Innovation Program for Quantum Science and Technology 2021ZD0302100. N.S. is supported by the European Union's Horizon 2020 program through the ERC-CoG SEQUAM (Grant No. 863476), and the Austrian Science Fund FWF (Grants No. P36305 and F7117).

-
- [1] J. I. Cirac, D. Pérez-García, N. Schuch, and F. Verstraete, Matrix product states and projected entangled pair states: Concepts, symmetries, theorems, *Rev. Mod. Phys.* **93**, 045003 (2021).
 - [2] M. C. Bañuls, Tensor network algorithms: A route map, *Annual Review of Condensed Matter Physics* **14**, 173 (2023).
 - [3] A. Banerjee, J. Yan, J. Knolle, C. A. Bridges, M. B. Stone, M. D. Lumsden, D. G. Mandrus, D. A. Tennant, R. Moessner, and S. E. Nagler, Neutron scattering in the proximate quantum spin liquid α -RuCl₃, *Science* **356**, 1055 (2017).
 - [4] C. Gross and I. Bloch, Quantum simulations with ultracold atoms in optical lattices, *Science* **357**, 995 (2017).
 - [5] F. Verstraete and J. I. Cirac, Renormalization algorithms for quantum-many body systems in two and higher dimensions, arXiv preprint (2004), [cond-mat/0407066](#).
 - [6] N. Schuch, I. Cirac, and D. Pérez-García, PEPS as ground states: Degeneracy and topology, *Annals of Physics* **325**, 2153 (2010).
 - [7] D. J. Williamson, N. Bultinck, M. Mariën, M. B. Şahinoğlu, J. Haegeman, and F. Verstraete, Matrix product operators for symmetry-protected topological phases: Gauging and edge theories, *Phys. Rev. B* **94**, 205150 (2016).
 - [8] A. Francuz and J. Dziarmaga, Determining non-abelian topological order from infinite projected entangled pair states, *Phys. Rev. B* **102**, 235112 (2020).
 - [9] M. Iqbal and N. Schuch, Entanglement order parameters and critical behavior for topological phase transitions and beyond, *Phys. Rev. X* **11**, 041014 (2021).
 - [10] P. Corboz, A. M. Läuchli, K. Penc, M. Troyer, and F. Mila, Simultaneous dimerization and SU(4) symmetry breaking of 4-color fermions on the square lattice, *Phys. Rev. Lett.* **107**, 215301 (2011).
 - [11] P. Corboz and F. Mila, Tensor network study of the Shastry-Sutherland model in zero magnetic field, *Phys. Rev. B* **87**, 115144 (2013).
 - [12] P. Corboz, M. Lajkó, K. Penc, F. Mila, and A. M. Läuchli, Competing states in the SU(3) Heisenberg model on the honeycomb lattice: Plaquette valence-bond crystal versus dimerized color-ordered state, *Phys. Rev. B* **87**, 195113 (2013).
 - [13] P. Corboz and F. Mila, Crystals of bound states in the magnetization plateaus of the Shastry-Sutherland model, *Phys. Rev. Lett.* **112**, 147203 (2014).
 - [14] J. Hasik, D. Poilblanc, and F. Becca, Investigation of the Néel phase of the frustrated Heisenberg antiferromagnet by differentiable symmetric tensor networks, *SciPost Phys.* **10**, 12 (2021).
 - [15] W.-L. Tu, E.-G. Moon, K.-W. Lee, W. E. Pickett, and H.-Y. Lee, Field-induced Bose-Einstein condensation and supersolid in the two-dimensional Kondo necklace, *Commun. Phys.* **5**, 130 (2022).
 - [16] W.-L. Tu, X. Lyu, S. R. Ghazanfari, H.-K. Wu, H.-Y. Lee, and N. Kawashima, Cubic ferromagnet and emergent $U(1)$ symmetry on its phase boundary, *Phys. Rev. B* **107**, 224406 (2023).
 - [17] N. Schuch, D. Poilblanc, J. I. Cirac, and D. Pérez-García, Resonating valence bond states in the PEPS formalism, *Phys. Rev. B* **86**, 115108 (2012).
 - [18] H.-Y. Lee, R. Kaneko, T. Okubo, and N. Kawashima, Gapless Kitaev spin liquid to classical string gas through tensor networks, *Phys. Rev. Lett.* **123**, 087203 (2019).
 - [19] J.-Y. Chen, L. Vanderstraeten, S. Capponi, and D. Poilblanc, Non-abelian chiral spin liquid in a quantum antiferromagnet revealed by an iPEPS study, *Phys. Rev. B* **98**, 184409 (2018).
 - [20] J.-Y. Chen, S. Capponi, A. Wietek, M. Mambrini, N. Schuch, and D. Poilblanc, SU(3)₁ chiral spin liquid on the square lattice: A view from symmetric projected entangled pair states, *Phys. Rev. Lett.* **125**, 017201 (2020).
 - [21] J. Hasik, M. Van Damme, D. Poilblanc, and L. Vanderstraeten, Simulating chiral spin liquids with projected entangled-pair states, *Phys. Rev. Lett.* **129**, 177201 (2022).
 - [22] Y. Xu, S. Capponi, J.-Y. Chen, L. Vanderstraeten, J. Hasik, A. H. Nevidomskyy, M. Mambrini, K. Penc, and D. Poilblanc, Phase diagram of the chiral SU(3) antiferromagnet on the kagome lattice, arXiv preprint (2023), [2306.16192](#).
 - [23] P. Corboz, T. M. Rice, and M. Troyer, Competing states in the t - J model: Uniform d -wave state versus stripe state, *Phys. Rev. Lett.* **113**, 046402 (2014).
 - [24] B.-X. Zheng, C.-M. Chung, P. Corboz, G. Ehlers, M.-P. Qin, R. M. Noack, H. Shi, S. R. White, S. Zhang, and G. K.-

- L. Chan, Stripe order in the underdoped region of the two-dimensional Hubbard model, *Science* **358**, 1155 (2017).
- [25] B. Ponsioen, S. S. Chung, and P. Corboz, Period 4 stripe in the extended two-dimensional Hubbard model, *Phys. Rev. B* **100**, 195141 (2019).
- [26] Q. Mortier, N. Schuch, F. Verstraete, and J. Haegeman, Tensor networks can resolve Fermi surfaces, *Phys. Rev. Lett.* **129**, 206401 (2022).
- [27] B. Ponsioen, S. S. Chung, and P. Corboz, Superconducting stripes in the hole-doped three-band Hubbard model, arXiv preprint (2023), 2306.12910.
- [28] L. Vanderstraeten, M. Mariën, F. Verstraete, and J. Haegeman, Excitations and the tangent space of projected entangled-pair states, *Phys. Rev. B* **92**, 201111 (2015).
- [29] L. Vanderstraeten, J. Haegeman, and F. Verstraete, Simulating excitation spectra with projected entangled-pair states, *Phys. Rev. B* **99**, 165121 (2019).
- [30] B. Ponsioen and P. Corboz, Excitations with projected entangled pair states using the corner transfer matrix method, *Phys. Rev. B* **101**, 195109 (2020).
- [31] B. Ponsioen, F. F. Assaad, and P. Corboz, Automatic differentiation applied to excitations with projected entangled pair states, *SciPost Phys.* **12**, 006 (2022).
- [32] R. Chi, Y. Liu, Y. Wan, H.-J. Liao, and T. Xiang, Spin excitation spectra of anisotropic spin-1/2 triangular lattice Heisenberg antiferromagnets, *Phys. Rev. Lett.* **129**, 227201 (2022).
- [33] A. Kshetrimayum, H. Weimer, and R. Orús, A simple tensor network algorithm for two-dimensional steady states, *Nature communications* **8**, 1 (2017).
- [34] P. Czarnik, J. Dziarmaga, and P. Corboz, Time evolution of an infinite projected entangled pair state: An efficient algorithm, *Phys. Rev. B* **99**, 035115 (2019).
- [35] J. Dziarmaga, Time evolution of an infinite projected entangled pair state: Neighborhood tensor update, *Phys. Rev. B* **104**, 094411 (2021).
- [36] C. Mc Keever and M. H. Szymańska, Stable iPEPO tensor-network algorithm for dynamics of two-dimensional open quantum lattice models, *Phys. Rev. X* **11**, 021035 (2021).
- [37] J. Dziarmaga, Time evolution of an infinite projected entangled pair state: A gradient tensor update in the tangent space, *Phys. Rev. B* **106**, 014304 (2022).
- [38] S.-H. Lin, M. P. Zaletel, and F. Pollmann, Efficient simulation of dynamics in two-dimensional quantum spin systems with isometric tensor networks, *Phys. Rev. B* **106**, 245102 (2022).
- [39] P. Czarnik, L. Cincio, and J. Dziarmaga, Projected entangled pair states at finite temperature: Imaginary time evolution with ancillas, *Phys. Rev. B* **86**, 245101 (2012).
- [40] P. Czarnik and P. Corboz, Finite correlation length scaling with infinite projected entangled pair states at finite temperature, *Phys. Rev. B* **99**, 245107 (2019).
- [41] A. Kshetrimayum, M. Rizzi, J. Eisert, and R. Orús, Tensor network annealing algorithm for two-dimensional thermal states, *Phys. Rev. Lett.* **122**, 070502 (2019).
- [42] D. Poilblanc, M. Mambrini, and F. Alet, Finite-temperature symmetric tensor network for spin-1/2 Heisenberg antiferromagnets on the square lattice, *SciPost Phys.* **10**, 019 (2021).
- [43] J. L. Jiménez, S. P. G. Crone, E. Fogh, M. E. Zayed, R. Lortz, E. Pomjakushina, K. Conder, A. M. Läuchli, L. Weber, S. Wessel, A. Honecker, B. Normand, C. Rüegg, P. Corboz, H. M. Rønnow, and F. Mila, A quantum magnetic analogue to the critical point of water, *Nature* **592**, 370 (2021).
- [44] A. Sinha, M. M. Rams, P. Czarnik, and J. Dziarmaga, Finite-temperature tensor network study of the Hubbard model on an infinite square lattice, *Phys. Rev. B* **106**, 195105 (2022).
- [45] B. Vanhecke, D. Devoogdt, F. Verstraete, and L. Vanderstraeten, Simulating thermal density operators with cluster expansions and tensor networks, *SciPost Phys.* **14**, 085 (2023).
- [46] S. Östlund and S. Rommer, Thermodynamic limit of density matrix renormalization, *Phys. Rev. Lett.* **75**, 3537 (1995).
- [47] J. Haegeman, B. Pirvu, D. J. Weir, J. I. Cirac, T. J. Osborne, H. Verschelde, and F. Verstraete, Variational matrix product ansatz for dispersion relations, *Phys. Rev. B* **85**, 100408 (2012).
- [48] R. P. Feynman, Atomic theory of the λ transition in helium, *Phys. Rev.* **91**, 1291 (1953).
- [49] R. P. Feynman, Atomic theory of liquid helium near absolute zero, *Phys. Rev.* **91**, 1301 (1953).
- [50] R. P. Feynman, Atomic theory of the two-fluid model of liquid helium, *Phys. Rev.* **94**, 262 (1954).
- [51] R. P. Feynman and M. Cohen, Energy spectrum of the excitations in liquid helium, *Phys. Rev.* **102**, 1189 (1956).
- [52] S. M. Girvin, A. H. MacDonald, and P. M. Platzman, Magneto-roton theory of collective excitations in the fractional quantum Hall effect, *Phys. Rev. B* **33**, 2481 (1986).
- [53] D. P. Arovas, A. Auerbach, and F. D. M. Haldane, Extended Heisenberg models of antiferromagnetism: Analogies to the fractional quantum Hall effect, *Phys. Rev. Lett.* **60**, 531 (1988).
- [54] J. Haegeman, T. J. Osborne, and F. Verstraete, Post-matrix product state methods: To tangent space and beyond, *Phys. Rev. B* **88**, 075133 (2013).
- [55] L. Vanderstraeten, J. Haegeman, and F. Verstraete, Tangent-space methods for uniform matrix product states, *SciPost Phys. Lect. Notes*, 7 (2019).
- [56] B. Buyens, J. Haegeman, K. Van Acoleyen, H. Verschelde, and F. Verstraete, Matrix product states for gauge field theories, *Phys. Rev. Lett.* **113**, 091601 (2014).
- [57] A. K. Bera, B. Lake, F. H. L. Essler, L. Vanderstraeten, C. Hubig, U. Schollwöck, A. T. M. N. Islam, A. Schneidewind, and D. L. Quintero-Castro, Spinon confinement in a quasi-one-dimensional anisotropic Heisenberg magnet, *Phys. Rev. B* **96**, 054423 (2017).
- [58] L. Vanderstraeten, M. Van Damme, H. P. Büchler, and F. Verstraete, Quasiparticles in quantum spin chains with long-range interactions, *Phys. Rev. Lett.* **121**, 090603 (2018).
- [59] V. Zauner-Stauber, L. Vanderstraeten, J. Haegeman, I. P. McCulloch, and F. Verstraete, Topological nature of spinons and holons: Elementary excitations from matrix product states with conserved symmetries, *Phys. Rev. B* **97**, 235155 (2018).
- [60] M. Van Damme, R. Vanhove, J. Haegeman, F. Verstraete, and L. Vanderstraeten, Efficient matrix product state methods for extracting spectral information on rings and cylinders, *Phys. Rev. B* **104**, 115142 (2021).
- [61] A. Milsted, J. Liu, J. Preskill, and G. Vidal, Collisions of false-vacuum bubble walls in a quantum spin chain, *PRX Quantum* **3**, 020316 (2022).
- [62] W. Kadow, L. Vanderstraeten, and M. Knap, Hole spectral function of a chiral spin liquid in the triangular lattice Hubbard model, *Phys. Rev. B* **106**, 094417 (2022).
- [63] M. Drescher, L. Vanderstraeten, R. Moessner, and F. Pollmann, Dynamical signatures of symmetry broken and liquid phases in an $s=1/2$ Heisenberg antiferromagnet on the triangular lattice, arXiv preprint (2022), 2209.03344.
- [64] W.-L. Tu, H.-K. Wu, N. Schuch, N. Kawashima, and J.-Y. Chen, Generating function for tensor network diagrammatic summation, *Phys. Rev. B* **103**, 205155 (2021).
- [65] J. Eisert, M. Cramer, and M. B. Plenio, Colloquium: Area laws for the entanglement entropy, *Rev. Mod. Phys.* **82**, 277 (2010).

- [66] A. Anshu, A. Harrow, and M. Soleimanifar, Entanglement spread area law in gapped ground states, *Nat. Phys.* **1**, 646 (2022).
- [67] M. Rader and A. M. Läuchli, Finite correlation length scaling in Lorentz-invariant gapless iPEPS wave functions, *Phys. Rev. X* **8**, 031030 (2018).
- [68] P. Corboz, P. Czarnik, G. Kapteijns, and L. Tagliacozzo, Finite correlation length scaling with infinite projected entangled-pair states, *Phys. Rev. X* **8**, 031031 (2018).
- [69] B. Vanhecke, J. Hasik, F. Verstraete, and L. Vanderstraeten, Scaling hypothesis for projected entangled-pair states, *Phys. Rev. Lett.* **129**, 200601 (2022).
- [70] J. Jordan, R. Orús, G. Vidal, F. Verstraete, and J. I. Cirac, Classical simulation of infinite-size quantum lattice systems in two spatial dimensions, *Phys. Rev. Lett.* **101**, 250602 (2008).
- [71] M. T. Fishman, L. Vanderstraeten, V. Zauner-Stauber, J. Haegeman, and F. Verstraete, Faster methods for contracting infinite two-dimensional tensor networks, *Phys. Rev. B* **98**, 235148 (2018).
- [72] L. Vanderstraeten, L. Burgelman, B. Ponsioen, M. Van Damme, B. Vanhecke, P. Corboz, J. Haegeman, and F. Verstraete, Variational methods for contracting projected entangled-pair states, *Phys. Rev. B* **105**, 195140 (2022).
- [73] M. Levin and C. P. Nave, Tensor renormalization group approach to two-dimensional classical lattice models, *Phys. Rev. Lett.* **99**, 120601 (2007).
- [74] Z. Y. Xie, H. C. Jiang, Q. N. Chen, Z. Y. Weng, and T. Xiang, Second renormalization of tensor-network states, *Phys. Rev. Lett.* **103**, 160601 (2009).
- [75] Z. Y. Xie, J. Chen, M. P. Qin, J. W. Zhu, L. P. Yang, and T. Xiang, Coarse-graining renormalization by higher-order singular value decomposition, *Phys. Rev. B* **86**, 045139 (2012).
- [76] R. J. Baxter, Variational approximations for square lattice models in statistical mechanics, *Journal of Statistical Physics* **19**, 461 (1978).
- [77] T. Nishino and K. Okunishi, Corner transfer matrix renormalization group method, *J. Phys. Soc. Jpn.* **65**, 891 (1996).
- [78] R. Orús and G. Vidal, Simulation of two-dimensional quantum systems on an infinite lattice revisited: Corner transfer matrix for tensor contraction, *Phys. Rev. B* **80**, 094403 (2009).
- [79] H. C. Jiang, Z. Y. Weng, and T. Xiang, Accurate determination of tensor network state of quantum lattice models in two dimensions, *Phys. Rev. Lett.* **101**, 090603 (2008).
- [80] H. N. Phien, J. A. Bengua, H. D. Tuan, P. Corboz, and R. Orús, Infinite projected entangled pair states algorithm improved: Fast full update and gauge fixing, *Phys. Rev. B* **92**, 035142 (2015).
- [81] L. Vanderstraeten, J. Haegeman, P. Corboz, and F. Verstraete, Gradient methods for variational optimization of projected entangled-pair states, *Phys. Rev. B* **94**, 155123 (2016).
- [82] P. Corboz, Variational optimization with infinite projected entangled-pair states, *Phys. Rev. B* **94**, 035133 (2016).
- [83] D. Poilblanc and M. Mambrini, Quantum critical phase with infinite projected entangled paired states, *Phys. Rev. B* **96**, 014414 (2017).
- [84] D. Poilblanc, Investigation of the chiral antiferromagnetic Heisenberg model using projected entangled pair states, *Phys. Rev. B* **96**, 121118 (2017).
- [85] H.-J. Liao, J.-G. Liu, L. Wang, and T. Xiang, Differentiable programming tensor networks, *Phys. Rev. X* **9**, 031041 (2019).
- [86] J. B. Rigo and A. K. Mitchell, Automatic differentiable numerical renormalization group, *Phys. Rev. Res.* **4**, 013227 (2022).
- [87] J. Haegeman, S. Michalakakis, B. Nachtergaele, T. J. Osborne, N. Schuch, and F. Verstraete, Elementary excitations in gapped quantum spin systems, *Phys. Rev. Lett.* **111**, 080401 (2013).
- [88] Considering larger patches is also possible, although comes with higher computational cost.
- [89] Y.-H. Chen, K. Hsu, W.-L. Tu, H.-Y. Lee, and Y.-J. Kao, Variational tensor network operator, *Phys. Rev. Res.* **4**, 043153 (2022).
- [90] H. W. J. Blöte and Y. Deng, Cluster Monte Carlo simulation of the transverse Ising model, *Phys. Rev. E* **66**, 066110 (2002).
- [91] W. Zheng, J. Oitmaa, and C. J. Hamer, Series studies of the spin- $\frac{1}{2}$ Heisenberg antiferromagnet at $t = 0$: Magnon dispersion and structure factors, *Phys. Rev. B* **71**, 184440 (2005).
- [92] A. Lüscher and A. M. Läuchli, Exact diagonalization study of the antiferromagnetic spin- $\frac{1}{2}$ Heisenberg model on the square lattice in a magnetic field, *Phys. Rev. B* **79**, 195102 (2009).
- [93] B. Dalla Piazza, M. Mourigal, N. B. Christensen, G. J. Nilsen, P. Tregenna-Piggott, T. G. Perring, M. Enderle, D. F. McMorrow, D. A. Ivanov, and H. M. Rønnow, Fractional excitations in the square-lattice quantum antiferromagnet, *Nature Physics* **11**, 62 (2015).
- [94] H. Shao, Y. Q. Qin, S. Capponi, S. Chesi, Z. Y. Meng, and A. W. Sandvik, Nearly deconfined spinon excitations in the square-lattice spin-1/2 Heisenberg antiferromagnet, *Phys. Rev. X* **7**, 041072 (2017).
- [95] R. Verresen, F. Pollmann, and R. Moessner, Quantum dynamics of the square-lattice Heisenberg model, *Phys. Rev. B* **98**, 155102 (2018).
- [96] M. Powalski, K. P. Schmidt, and G. S. Uhrig, Mutually attracting spin waves in the square-lattice quantum antiferromagnet, *SciPost Phys.* **4**, 001 (2018).
- [97] S. Morita, R. Kaneko, and M. Imada, Quantum spin liquid in spin $1/2$ J_1 - J_2 Heisenberg model on square lattice: many-variable variational Monte Carlo study combined with quantum-number projections, *Journal of the Physical Society of Japan* **84**, 024720 (2015).
- [98] W.-Y. Liu, J. Hasik, S.-S. Gong, D. Poilblanc, W.-Q. Chen, and Z.-C. Gu, Emergence of gapless quantum spin liquid from deconfined quantum critical point, *Phys. Rev. X* **12**, 031039 (2022).
- [99] L. Wang and A. W. Sandvik, Critical level crossings and gapless spin liquid in the square-lattice spin-1/2 $J_1 - J_2$ Heisenberg antiferromagnet, *Phys. Rev. Lett.* **121**, 107202 (2018).
- [100] F. Ferrari and F. Becca, Spectral signatures of fractionalization in the frustrated Heisenberg model on the square lattice, *Phys. Rev. B* **98**, 100405 (2018).
- [101] V. Zauner-Stauber, L. Vanderstraeten, J. Haegeman, I. P. McCulloch, and F. Verstraete, Topological nature of spinons and holons: Elementary excitations from matrix product states with conserved symmetries, *Phys. Rev. B* **97**, 235155 (2018).
- [102] L. Vanderstraeten, E. Wybo, N. Chepiga, F. Verstraete, and F. Mila, Spinon confinement and deconfinement in spin-1 chains, *Phys. Rev. B* **101**, 115138 (2020).
- [103] B. Ponsioen, J. Hasik, and P. Corboz, Improved summations of N-point correlation functions of projected entangled-pair states, arXiv preprint (2023), 2306.13327.